Magnetic, kinetic, and optical properties of new high-pressure phases in the system Cr–GaSb: Ab initio density functional theory study

ARTICLE *in* INTERNATIONAL JOURNAL OF QUANTUM CHEMISTRY · MARCH 2013

Impact Factor: 1.43 · DOI: 10.1002/qua.24097

6 AUTHORS, INCLUDING:

Erkin Kulatov
Russian Academy of Sciences
82 PUBLICATIONS **792** CITATIONS
SEE PROFILE

Maria Magnitskaya
Russian Academy of Sciences
20 PUBLICATIONS **155** CITATIONS
SEE PROFILE

V. Brazhkin
Russian Academy of Sciences
303 PUBLICATIONS **3,356** CITATIONS
SEE PROFILE

Magnetic, Kinetic, and Optical Properties of New High-Pressure Phases in the System Cr–GaSb: *Ab Initio* Density Functional Theory Study

Erkin Kulatov,[a] Maria Magnitskaya,*[b] Yurii Uspenskii,[c] Svetlana Popova,[b] Vadim Brazhkin,[b] and Evgenii Maksimov†[c]

The structural, transport, magnetic, and optical properties of high-pressure-synthesized metastable compounds CrGaSb and $CrGa_2Sb_2$ are calculated from first principles. In addition to theoretical results, new X-ray structural measurements of $CrGa_2Sb_2$ up to 9 GPa are reported. Both high-pressure phases CrGaSb and $CrGa_2Sb_2$ are found to be at the edge between metal and semiconductor, which implies that the standard density functional theory predictions may be misleading. To clarify the situation, a study is conducted whether the results depend significantly on the approximation used for the exchange–correlation potential. A possible effect of slight nonstoichiometry found in the $CrGa_2Sb_2$ samples is also investigated. The calculation results agree with most available experimental data and are internally consistent, which provides the assurance that, as a whole, they give a reliable picture of electronic properties in CrGaSb and $CrGa_2Sb_2$. © 2012 Wiley Periodicals, Inc.

DOI: 10.1002/qua.24097

Introduction

The design, fabrication, and study of new spintronics-related materials are of crucial importance for future technological applications. To integrate easily with existing electronic devices, such materials should combine room-temperature ferromagnetism with semiconducting or half-metallic properties.[1] Most investigations in this field have been devoted to the systems based on group-IV, III–V, and II–VI semiconductors doped with 3d-transition metals. Two types of such materials that attract major attention – diluted magnetic semiconductors (DMSs) and digital magnetic heterostructures (DMHs)[2,3] – are typically obtained using the molecular-beam epitaxy. Another promising method to create materials of this class is high-pressure synthesis from constituents. This method has been successfully applied to produce many novel compounds that remain metastable at atmospheric pressure, but cannot be obtained directly at normal conditions.

The systems *M*–GaSb (*M* is a magnetic 3d element) are attractive as a possible basis for designing spintronics-related materials, since they contain magnetic (*M*) and semiconducting (GaSb) components. Recently, two previously unknown compounds in the system Mn–GaSb have been synthesized under high-pressure/temperature conditions. One of them with the chemical formula $MnGa_2Sb_2$ crystallizes in an orthorhombic structure,[4–6] while another phase with the composition MnGaSb has a tetragonal structure.[4,5] Both phases are metallic and ferromagnetic (FM). More recently, an orthorhombic high-pressure phase $CrGa_2Sb_2$ closely similar to $MnGa_2Sb_2$ has been synthesized at pressures from 6 to 8 GPa and temperatures from 700 to 900 K.[7,8] A tetragonal phase CrGaSb isostructural to MnGaSb has been also obtained[8] at higher synthesis temperatures. Contrary to its Mn-based analogue, the phase CrGaSb is paramagnetic from 4.2 to 300 K.[8] These four compounds are metastable at ambient conditions.

Among them, the compound $CrGa_2Sb_2$ is considered[8] as promising for future spintronics applications, because it exhibits above-room-temperature ferromagnetism (the Curie temperature $T_C \sim 345$–350 K)[7,8] and has a very high electrical resistivity, which might be an evidence of semiconducting properties.[8] According to Ref. [7], this compound is slightly non-stoichiometric, with the exact chemical formula $Cr_{0.9585}Ga_2Sb_2$, that is, it contains about 4% of Cr vacancies. Notice that structural defects and residual microstresses typical of nonequilibrium metastable phases may lead to uncertainties in the experimental results. In this situation, first-principles calculations are growing in importance because they provide information independent of experiment.

In this article, we present *ab initio* density functional theory (DFT) calculations of $CrGa_2Sb_2$, (both with and without Cr

[a] *E. Kulatov*
A.M. Prokhorov General Physics Institute, Russian Academy of Sciences, 119991 Moscow, Russia
[b] *M. Magnitskaya, S. Popova, V. Brazhkin*
Institute for High Pressure Physics, Russian Academy of Sciences, 142190 Troitsk, Moscow Region, Russia
E-mail: magnma@gmail.com
[c] *Y. Uspenskii, E. Maksimov†*
P.N. Lebedev Physical Institute, Russian Academy of Sciences, 119991 Moscow, Russia
†Diseased

Contract grant sponsors: Ministry of Education and Science of Russia, Russian Academy of Sciences, and Russian Foundation for Basic Research; Contract grant numbers: 10-02-00118, 10-02-00694, 10-02-00698, and 11-02-00615.

vacancies) and, for the sake of comparison, of CrGaSb. Part of the calculation results have been briefly reported in Ref. [9]. Here, the calculated structural, electronic and magnetic properties are compared with available experimental data.[7,8] We also present optical and magneto-optical (MO) spectra of $CrGa_2Sb_2$ and CrGaSb, which are still not measured experimentally. The effect of different exchange–correlation potentials on the electronic structure of $CrGa_2Sb_2$ is studied in detail. In addition, new experimental data on the lattice parameters and equation of state of $CrGa_2Sb_2$ in the pressure range up to 9 GPa are presented.

Calculation Method

Our first-principles calculations are based on the DFT formalism.[10] The full-potential relativistic augmented plane-wave plus local-orbital method as implemented in WIEN2k code[11] is applied. The conductivity measurements[8] suggest that the phases CrGaSb and $CrGa_2Sb_2$ are at the border between metals and semiconductors, which provides a significant challenge for DFT predictions. In this case, one should pay particular attention to the notorious "gap problem," because errors in evaluating the band gaps may qualitatively affect the results. For this reason, we made calculations using three different approximations for the exchange–correlation potential V_{xc}: the local spin-density approximation (LDA) proposed by Ceperley–Alder[12] and reparameterized by Perdew–Wang (PW-92),[13] the generalized gradient approximation (GGA) in the form proposed by Perdew–Burke–Ernzerhof (PBE-96),[14] and a simple modification of Becke–Johnson (BJ)[15] potential (used in combination with the PW-92 correlation) recently proposed by Tran–Blaha.[16] Most calculations reported below are made using the PBE-96 approximation. As is known, GGA functionals, such as PBE, perform well for the equilibrium geometry and energetics. However, they underestimate band gaps and may overestimate magnetic moments compared to LDA. The modified BJ (MBJ) exchange–correlation potential, semilocal as it is, yields band gaps with an accuracy comparable to orbital-dependent hybrid functionals, which are at least one order of magnitude more computationally expensive.[16] The MBJ approximation includes, to some extent, many-particle effects, thus improving[16,17] the DFT-LDA/GGA band gaps and magnetic moments in semiconductors and half-metallic ferromagnets. So, we also calculate the electronic and magnetic properties using the MBJ exchange–correlation potential.

The inclusion of spin-orbit (SO) coupling effects is essential for calculating MO spectra and particularly important for the system under study because of the presence of the relatively heavy Sb atoms. The SO coupling was included self-consistently by solving the radial Dirac equation for the core electrons and evaluated by the second-variation method[18] using scalar relativistic eigenvectors for the valence states. As the SO coupling is large only near the core, the corresponding contributions to the Hamiltonian are only evaluated inside the muffin-tin (MT) spheres. The MT-radii R of Cr, Ga, and Sb were set to 2.50, 2.32, and 2.39 Bohr, respectively. The energy cut-off $E_{cut} = K_{max}^2$ was equal to 162 eV. The maximal number of **k** points, 2236 in the irreducible 1/4 part of the Brillouin zone (BZ), was used for the phase $CrGa_2Sb_2$. Note that the use of a smaller number of **k** points (1118) did not markedly change both the ground state properties and the optical and MO spectra. The calculations were performed at the experimental lattice periods.[7,8] Starting from the experimental atomic positions, we did the geometry relaxation to allow the internal atomic coordinates to change, until the residual atomic forces were converged down to 6 meV/Å. The convergence of charge density was better than 0.001 of electron charge.

To investigate the effect of small (4.15%) Cr deficiency reported[7] for $CrGa_2Sb_2$, we also made calculations for the 1 × 2 × 2 supercell with 6.25% of Cr vacancies, which models a hypothetical nonstoichiometric compound $Cr_{0.9375}Ga_2Sb_2$ (below it is approximately denoted as $Cr_{0.94}Ga_2Sb_2$). Based on the optimized crystal structures, the physical properties of CrGaSb, $CrGa_2Sb_2$, and $Cr_{0.94}Ga_2Sb_2$ were evaluated.

Previously, we successfully used this approach for DFT calculations of new high-pressure-synthesized FM Ca–3d metal Laves phases,[19] as well as for an extensive first-principles study of the DMSs and DMHs based on group-IV and III–V semiconductors doped with magnetic 3d-metals.[20] In particular, the first-principles calculations[20] have shown the solid solution of Cr in GaSb matrix to be FM.

Calculation Results for CrGaSb, $CrGa_2Sb_2$, and $Cr_{0.94}Ga_2Sb_2$

Crystal structures

Because of inhomogeneities inherent in nonequilibrium high-pressure phases, the identification of their crystal structure and exact composition is sometimes a challenging issue. For example, $MnGa_2Sb_2$ was first erroneously solved[4] as a simple cubic structure. As is noted in Ref. [8], the Mn-based orthorhombic phase, in contrast to $CrGa_2Sb_2$, is probably a set of solid solutions. This results in the sensitivity of experimental data to variations of composition that depends on synthesis conditions. Initially, the high-pressure phase CrGaSb has been identified[8] as a tetragonal structure of the $CuAl_2$-type (space group I4/mcm, No. 140) with the lattice periods $a = 6.466$ Å and $c = 5.291$ Å, $c/a = 0.82$. The point is that Ga and Sb atoms are practically indistinguishable for the X-ray diffraction analysis, so the ternary CrGaSb is seen as a binary with the $CuAl_2$-type structure having an inversion center. If one makes a distinction between the Ga and Sb sites, the structure of CrGaSb must be noncentrosymmetric. The symmetry analysis of measured[8] atomic positions allows for CrGaSb two alternative structures, monoclinic P2/m (SG No. 6), and tetragonal P4bm (SG No. 100), each containing four formula units per elementary cell. Looking along the c-axis, the monoclinic P2/m structure can be seen as a stack of metallic Cr planes sandwiched by the Ga–Sb ones (Fig. 1a), while the tetragonal P4bm structure is composed of alternate Cr, Ga, Cr, Sb layers (Fig. 1b). If the Ga and Sb sites were occupied with identical atoms, the structure in Figure 1b would be of the $CuAl_2$ type. All the subsequent calculations of CrGaSb are performed for

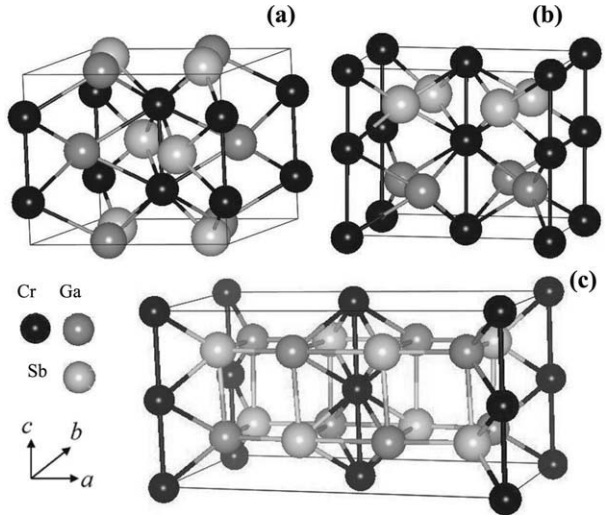

Figure 1. a) The monoclinic P2/m and b) tetragonal P4bm structures of the phase CrGaSb: P4bm structure is energetically more preferable. c) The BCO Iba2 structure of $CrGa_2Sb_2$.

the P4bm structure, which is lower in energy (by 0.137 eV/f.u.) than the monoclinic P2/m structure.

The high-pressure phase $CrGa_2Sb_2$ has a body-centered orthorhombic (BCO) structure (space group Iba2, No. 45),[7,8] whose elementary cell containing four formula units is shown in Figure 1c (not to be confused with primitive cell that contains 2 f.u.). In the Iba2 structure, the arrangement of metallic Cr planes along the *a*-axis is somewhat similar to that of P4bm structure, with the difference that these planes are sandwiched with eight nontransition atoms instead of four. To our knowledge, the P4bm and Iba2 structures were not previously observed for ternary compounds.

The measured[8] lattice parameters of $CrGa_2Sb_2$ ($a = 11.772$ Å, $b = 5.964$ Å, and $c = 5.897$ Å) are very close to those reported in Ref. [7] (11.781, 5.968, and 5.902 Å, respectively). Based on the relaxed atomic positions, the interatomic distances and bond angles for $CrGa_2Sb_2$ were evaluated. Some of them listed in Table 1 demonstrate very good agreement with the experimental data.[7] The $1 \times 2 \times 2$ supercell used to evaluate the effect of Cr deficiency, contains four elementary cells shown in Figure 1c, that is, 16 f.u. The nonstoichiometric compound $Cr_{0.94}Ga_2Sb_2$ was modeled by removing one of 16 Cr atoms.

Table 1. Selected interatomic distances and bond angles for $CrGa_2Sb_2$.

	Experiment[a]	This work
Distance (Å)		
Cr—Cr	2.951	2.951
Cr—Ga	2.627	2.647
Cr—Sb	2.736	2.724
Angle (°)		
Cr—Cr—Cr	180.0	180.0
Ga—Cr—Ga	109.93	112.25
Sb—Cr—Sb	115.27	114.42
Ga—Cr—Sb	70.84	70.94

[a] Ref. [7].

The equation of state of $CrGa_2Sb_2$: Theory and experiment

In this section, we present the results of X-ray measurements of lattice parameters for $CrGa_2Sb_2$ under compression up to 9 GPa. For detailed description of high-pressure synthesis and structure identification see Ref. [8] and references therein. Here, we only mention that the experimental samples were obtained by quenching from the melt (synthesis temperatures in the range 700–900 K) to room temperature in Toroid anvils[21] under the synthesis pressures in the range 6–8 GPa.

The *in situ* structural study of synthesized crystalline $CrGa_2Sb_2$ under pressure was performed by the energy-dispersive X-ray diffraction method in the SMAP-180 press machine at the BL14B1 beam-line of SPring-8. Cylinder-shaped samples were produced by pressing from a polycrystalline powder of 10–20 μm in grain size. The samples were placed in a container from either hexagonal BN or high-purity graphite. A cubic press was used for generating high-pressures of up to 9 GPa. During measurements, the energy-dispersive Canberra detector (the energy range for a white beam was 5–150 keV) was kept at fixed angles $2\theta = 6^\circ$ and $2\theta = 3^\circ$. The energy range of the detection of scattered photons for the reflections from a particular $CrGa_2Sb_2$ sample under pressure was roughly 30–110 keV, which corresponded to the scattering wave-vectors Q approximately from 1.6 to 5.6 Å^{-1} ($Q = 2\pi/d$, where d is an interplanar spacing of diffraction). Reflections for $CrGa_2Sb_2$ were reliably detected and identified in the Q range from 1.8 to 4.8 Å^{-1}.

The experimental dependence $P(V)$ is presented in Figure 2 along with the theoretical equation of state. The latter is found

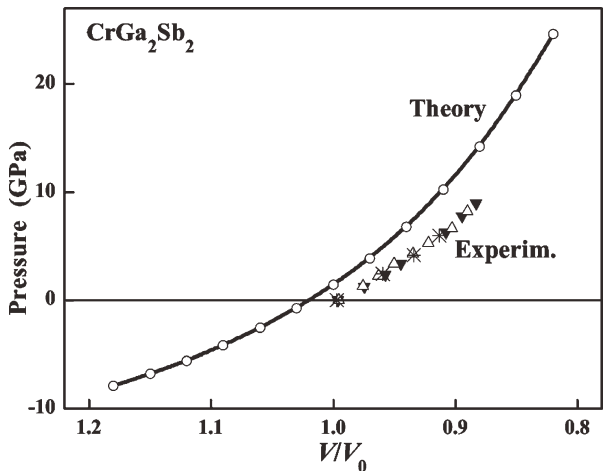

Figure 2. Calculated (the line with circles) and measured (stars and triangles) equation of state for $CrGa_2Sb_2$. Different symbols refer to the experimental data obtained in different ways (see text). The abscissa is the relative volume V/V_0, where V_0 is the experimental volume at $P = 0$.

as $P(V) = -\partial E_{tot}(V)/\partial V$ from the Birch–Murnaghan fit to the calculated total energy E_{tot} as a function of volume. In Figure 2, the theoretical curve $P(V/V_0)$, where V_0 is the experimental volume at normal pressure, is displayed by solid line with open circles, and other symbols present our experimental data obtained by different methods. The open and closed triangles

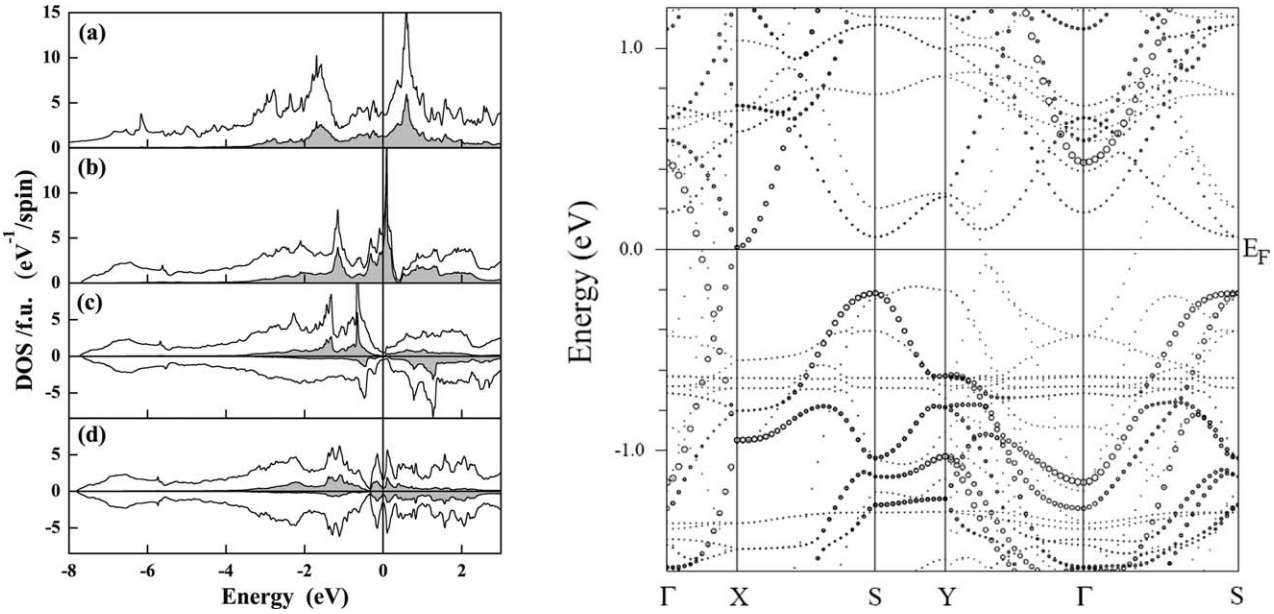

Figure 3. (left) Spin projected total DOS (solid lines) for a) NM tetragonal CrGaSb, b) NM, c) ferromagnetic and d) AFM phases of $CrGa_2Sb_2$; shaded regions correspond to the partial DOS of Cr 3d-states. Energy is measured from the Fermi level E_F. (right) Band structure of FM $CrGa_2Sb_2$ along the high-symmetry lines of BZ. Sizes of circles are determined by the contribution of Sb 5p-states.

refer to the measurements on previously synthesized samples of $CrGa_2Sb_2$, with increasing and decreasing pressure, respectively. The stars indicate the data obtained on decompression of the phase $CrGa_2Sb_2$ synthesized *in situ* from a powder mixture of pure Cr and GaSb. The calculated equilibrium volume per formula unit equal to 105.7 Å^3, is by ~2% larger than the experimental value[7] of 103.5 Å^3. The $P = 0$ bulk modulus $B = -V(\partial P/\partial V)$ and its pressure derivative $B' = \partial B/\partial P$ are equal to 71.0 GPa and 4.0, respectively, while the corresponding experimental values are 67 (±6) GPa and 3.1.

Electronic structure and magnetic properties

Figures 3a–3d display the spin-polarized and nonspin-polarized density of states (DOS). The shaded area presents the Cr 3d-states contribution. Our calculations for the tetragonal phase CrGaSb reveal a lack of magnetic solution, in accordance with experiment[8] (Fig. 3a). Figure 3b presents the DOS of nonmagnetic (NM) orthorhombic $CrGa_2Sb_2$, whose Fermi level, E_F, falls on a high peak of $N(E)$ formed by Cr 3d-states slightly hybridized with Ga and Sb p-states. The DOS of FM state of BCO $CrGa_2Sb_2$ around E_F is much lower in than in the NM case and contributed mostly by the hybridized Ga and Sb p-states (Fig. 3c). A lower value of DOS at E_F means that the FM state of $CrGa_2Sb_2$ is energetically preferable over the NM state and, indeed, its total energy is by ~0.43 eV/f.u. lower than in the NM case. The partial Cr 3d-DOS of FM $CrGa_2Sb_2$ exhibits an exchange splitting of 2 eV for the t_{2g} states of *xz* and *yz* symmetries, which appreciably exceeds a crystal-field splitting between the e_g and t_{2g} bands (~0.7–0.8 eV). The comparison of DOS's at E_F also reveals a large preference of the FM state over the anti-FM (AFM) one (Fig. 3d). The total energy calculation supports this expectation: $E_{AFM} - E_{FM} = +0.22$ eV/f.u. This large energy gain correlates with the high Curie temperature $T_C \sim 345$–350 K measured[7,8] for $CrGa_2Sb_2$.

The most striking feature of DOS in the case of FM $CrGa_2Sb_2$ is a pseudogap around E_F typical of poor metals. The band structure diagram [Fig. 3 (right)] shows that a real bandgap exists along the high-symmetry directions *S–X* and *S–Y* of the first BZ, while in other directions (Γ–*X*, Γ–*Y*, and Γ–*S*) there are bands crossing E_F. These bands have large dispersion and hence produce a low DOS at the Fermi level, $N(E_F)$ (for convenience sake the band structure of $CrGa_2Sb_2$ shown in Figure 3 (right) was calculated for the artificially doubled BCO unit cell shown in Figure 1c, a new cell being a rectangular parallelepiped). However, $CrGa_2Sb_2$ is not semiconducting as has been suggested in Ref. [8] on the basis of conductivity measurements. Notice that the band structure in Figure 3 (right) is calculated with the inclusion of SOC term, which mixes spin-up and spin down states, such that they cannot be distinguished in figure.

The total equilibrium magnetic moment of $CrGa_2Sb_2$ is $M_{tot} = 1.96\ \mu_B$ per one Cr atom. Its main spin constituents are $M_{Cr} = +2.03\ \mu_B$, $M_{Sb} = -0.05\ \mu_B$, and $M_{Ga} = -0.004\ \mu_B$. A contribution of orbital moments is negligible: $M_{tot}^{orb} = -0.005\ \mu_B$, $M_{Cr}^{orb} = -0.006\ \mu_B$, $M_{Sb}^{orb} = +0.0008\ \mu_B$, and $M_{Ga}^{orb} = +0.0003\ \mu_B$. An alternative way for evaluating the magnetic properties is the fixed-spin-moment (FSM) technique.[22] As is seen in Figure 4a, this procedure produces for $CrGa_2Sb_2$ only one stable solution at $M_{tot} \sim 2\ \mu_B$/Cr. An energy gain of FM solution over the NM one is ΔE ~0.41 eV/f.u. Both the values of ΔE and M_{tot} are very close to those obtained in our conventional spin-polarized calculation. So, our results on electronic and magnetic properties of $CrGa_2Sb_2$ are internally consistent.

However, the experiment[7] provides a saturation magnetic moment $M = 1.6\ \mu_B$/Cr (extrapolated to 0 K) and a

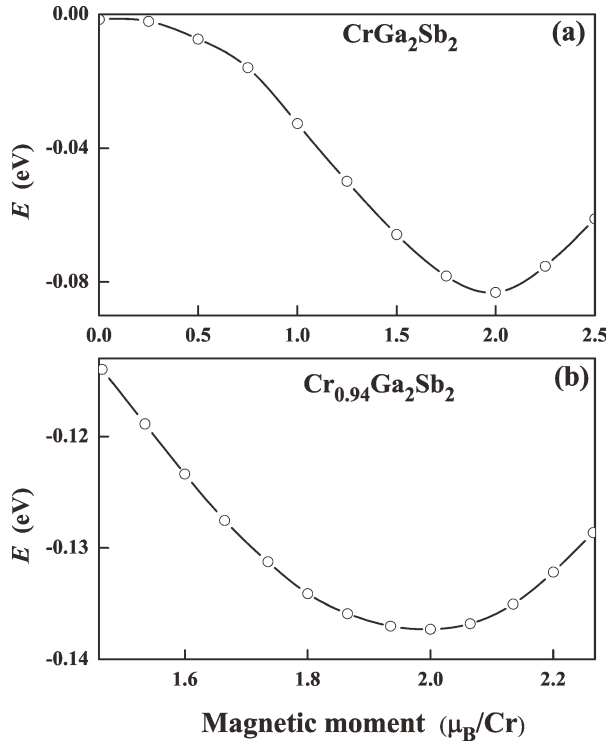

Figure 4. FSM diagram for (a) perfect and (b) Cr-deficient $CrGa_2Sb_2$.

paramagnetic moment of 2.4 μ_B/Cr (above the Curie temperature). An even lower value of $M = 1.35$ μ_B/Cr is found in Ref. [8]. Assuming that the lower experimental values of M can be related to the Cr vacancies present in the experimental samples, we applied the FSM procedure to the nonstoichiometric compound $Cr_{0.94}Ga_2Sb_2$. In this case, the FM solution is also strongly preferable (Fig. 4b) and an average magnetic moment is even higher (2.05 μ_B/Cr) than for stoichiometric $CrGa_2Sb_2$ (Table 2). A negligible difference in magnetic properties

Table 2. Magnetic moment of $CrGa_2Sb_2$ in different approximations.

Method	Magnetic moment (μ_B/Cr)	
Experiment	1.6[a]	1.35[b]
LDA	1.92	1.8[c]
GGA	1.96	2.05[d]
MBJ	2.02	–

[a] Ref. [7]. [b] Ref. [8]. [c] $P = 9$ GPa. [d] 6% of Cr vacancies.

between $CrGa_2Sb_2$ and $Cr_{0.94}Ga_2Sb_2$ implies that the smaller observed[7,8] magnetic moment compared to the calculated one cannot be explained by the presence of Cr vacancies. This discrepancy may be ascribed to residual microstresses, chemical disorder, and other structural defects that may exist in metastable high-pressure phases. Incidentally, the magnetic moment of experimental samples with Cr content increased by 20% is lower than for the stochiometric $CrGa_2Sb_2$ phase.[8] This fact has been attributed[8] to the possible formation of AFM precipitates of excess Cr, resulting in a reduced value of measured magnetic moment.

The effect of different factors on the electronic and magnetic properties of $CrGa_2Sb_2$ is illustrated in Figure 5 and Table 2, respectively. Knowing that the GGA magnetic moments can be overestimated in comparison with the LDA ones, we performed LSDA (PW-92) calculations for $CrGa_2Sb_2$. Having in mind that metastable high-pressure phases are nonequilibrium at normal conditions and that application of high-pressure suppresses magnetic properties, we made the LDA calculations of $CrGa_2Sb_2$ at relative volume $V/V_0 = 0.91$ corresponding to the experimental pressure of 9 GPa. If the electronic and magnetic properties of $CrGa_2Sb_2$ were sensitive to small variations in the cell volume, the calculation results would appreciably depend on the choice of initial structural parameters (recall that our calculations were made with the experimental[7] lattice periods). However, on compression to 9 GPa the magnetic moment was reduced only by ~6%, while the DOS at E_F practically did not change. Figure 5a presents the total (spin up + spin down) LDA DOSs of FM $CrGa_2Sb_2$ near the Fermi level. In the LDA case, at normal pressure as well as 9 GPa, $N(E_F)$ becomes higher, with the pseudogap less pronounced, than for the GGA DOS (full line in Fig. 5b). The LDA magnetic moment M is only 2% smaller than the GGA value, with further reduction of about 6% at 9 GPa. The dashed line in Figure 5b describes the total GGA DOS of FM $Cr_{0.94}Ga_2Sb_2$. It is seen that in the nonstoichiometric case the DOS is smoothed and shifted toward higher energies, with the result that $N(E_F)$ becomes three times larger than in the perfect compound $CrGa_2Sb_2$.

Application of the new MBJ exchange–correlation potential[16] again resulted in $M = 2.02$ μ_B/Cr. Thus, the magnetic moment of $CrGa_2Sb_2$ is not very sensitive to small nonstoichiometry and to the type of exchange–correlation potential. It is noteworthy that the magnetic moment of $CrGa_2Sb_2$ is very close to integer number 2. Considering the DOSs of $CrGa_2Sb_2$ in the order LDA–GGA–MBJ (Fig. 5c), one can see that $N(E_F)$ becomes smaller and pseudogap wider, however, $CrGa_2Sb_2$ is still not semiconducting. Figures 5d and 5e present the spin-projected DOS of FM $CrGa_2Sb_2$ obtained with GGA and MBJ functionals, respectively. With the MBJ potential $N(E_F)$ is by a factor of 1.8 lower than in the GGA case. Interestingly, in the MBJ calculation the DOS of spin-up electrons at 0.2 eV above E_F is nearly zero. If due to some reason (doping, disorder, compression, etc.) the Fermi level of $CrGa_2Sb_2$ was at this energy, this compound might possess half-metallic properties. This observation is consistent with the close to integer magnetic moment $M \approx 2$ μ_B/Cr in $CrGa_2Sb_2$, which is typical of half-metallic ferromagnets.

As is seen from the above, our results are stable against variations of the exchange–correlation potential. To understand the origin of this stability, we evaluated the degree of nonlocality of the self-energy within the *GW* approximation[23] $\Sigma_{xc}(\mathbf{r}, \mathbf{r}', E) \approx (i/2\pi)\int d\omega\, G(\mathbf{r}, \mathbf{r}', E - \omega)W(\mathbf{r}, \mathbf{r}', \omega)$. The nonlocality is largely determined by the static screened Coulomb interaction $W(\mathbf{r}, \mathbf{r}', 0)$, the latter rapidly decreasing over the distance $|\mathbf{r} - \mathbf{r}'| \geq r_{TF}$. Here, the Thomas–Fermi screening length r_{TF}, when averaged over the unit cell, is given by formula

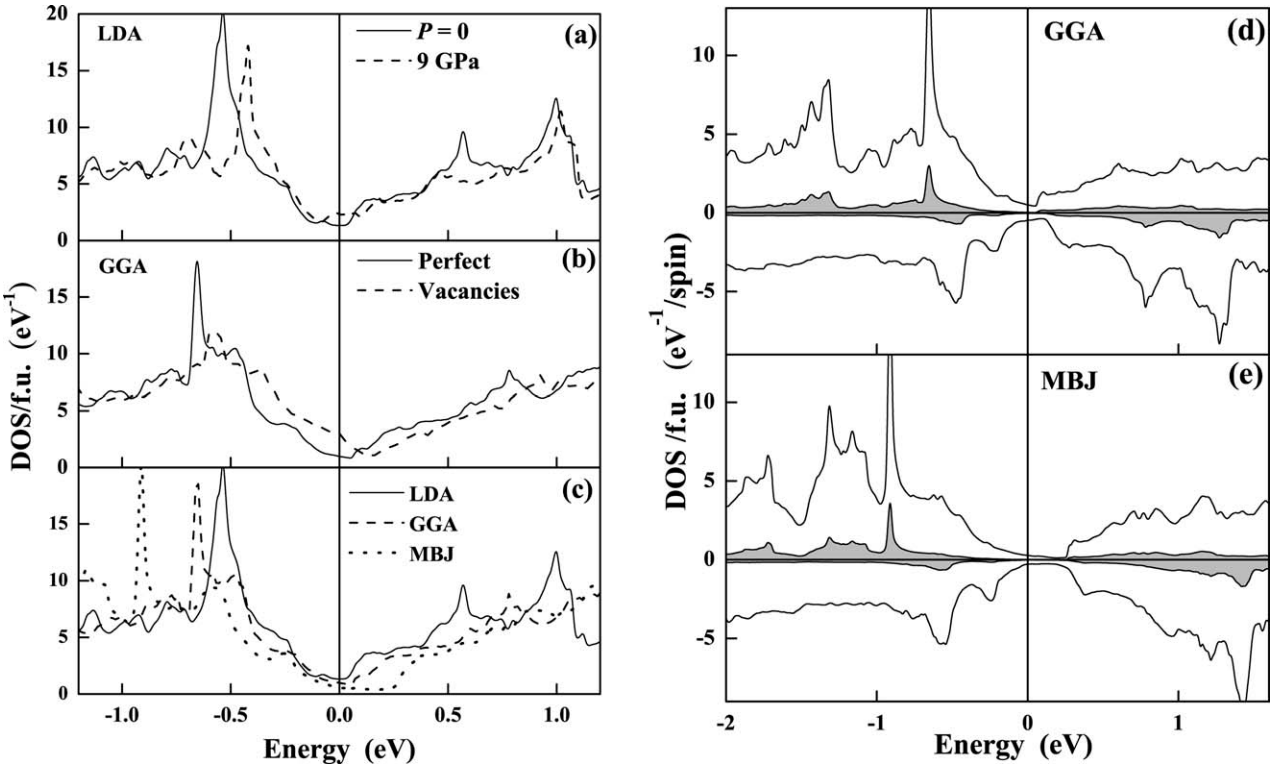

Figure 5. (left) Total (spin up + spin down) DOS of FM $CrGa_2Sb_2$, obtained with different exchange–correlation potentials. a) LDA at normal pressure (solid line) and $P = 9$ GPa (dashed line); b) GGA for $CrGa_2Sb_2$ (solid line) and $Cr_{0.94}Ga_2Sb_2$ (dashed line); c) comparison of LDA, GGA, and MBJ cases (solid, dashed and dotted lines, respectively). Energy is measured from the Fermi level E_F. (right) Spin-projected DOS for (d) GGA and (e) MBJ approximations. Gray regions correspond to the partial DOS of Cr 3d-states. Notice a half-metallic feature of the MBJ DOS slightly above E_F.

$$r_{TF} = \sqrt{\frac{V}{4\pi e^2 N(E_F)}}. \quad (1)$$

Semiconductors exhibit a long-range behavior of W and Σ_{xc}. As a result, their properties may significantly deviate from DFT predictions (a well-known example is an underestimation of band gaps in DFT calculations). According to (1), r_{TF} of $CrGa_2Sb_2$, even in the case of MBJ potential, is rather short, only ~1 Å, that is less than one-half of the nearest-neighbor distance of ~2.6 Å (Table 1). Thus, both $W(\mathbf{r}, \mathbf{r}', 0)$ and $\Sigma_{xc}(\mathbf{r}, \mathbf{r}', E)$ in $CrGa_2Sb_2$ have a short-range behavior, which is typical of metals.

Electrical conductivity and optical spectra

Below we present calculated optical spectra of CrGaSb, $CrGa_2Sb_2$, and $Cr_{0.94}Ga_2Sb_2$. Although there exist no experimental data to compare with, these calculations nevertheless provide rich information on the electronic structure and related properties. For instance, the tetragonal crystal structure of CrGaSb is not appreciably anisotropic (Fig. 1), while the BCO structure of $CrGa_2Sb_2$ possesses significant anisotropy (the *a*:*b*:*c* ratio of lattice parameters is approximately 2:1:1), which, as indicated later in this section, is reflected in both transport and optical properties.

We calculated the dielectric tensor $\varepsilon_{\alpha\beta}(\omega) = \varepsilon_{1,\alpha\beta}(\omega) + i\varepsilon_{2,\alpha\beta}(\omega)$ using the Drude expression and the random-phase approximation for intraband and interband contributions, respectively:

$$\varepsilon_{\alpha\beta}(\omega) = 1 - \frac{\omega^2_{p,\alpha\beta}}{\omega(\omega + i\gamma)} + \frac{4\pi e^2\hbar^2}{m^2 V}\sum_{i<f}\int_{BZ} d\mathbf{k}\frac{p_\alpha^{i,f}(\mathbf{k})p_\beta^{f,i}(\mathbf{k})[n_f(\mathbf{k}) - n_i(\mathbf{k})]}{E^2_{f,i}(\mathbf{k})[\hbar\omega - E_{f,i}(\mathbf{k}) + i\delta]}. \quad (2)$$

Here, the Greek subscripts indicate Cartesian components. In the interband contribution, m and e are the electronic mass and charge; V is the cell volume; $p_\alpha^{i,f}(\mathbf{k})$ is an α-component of the momentum operator matrix element taken between the states of ith (initial) and fth (final) bands; $E_{i(f)}(\mathbf{k})$ and $n_{i(f)}(\mathbf{k})$ are energies and occupation numbers in the $i(f)$th electron band; $E_{f,i}(\mathbf{k}) = E_f(\mathbf{k}) - E_i(\mathbf{k})$. The parameters of intraband contribution are the relaxation rate of Fermi electrons γ and the tensor of squared plasma frequency $\omega^2_{p,\alpha\beta}$ determined via integration over the Fermi surface:

$$\omega^2_{p,\alpha\beta} = \frac{4\pi e^2}{V}\sum_n \int_{BZ} d\mathbf{k} v_\alpha^n(\mathbf{k}) v_\beta^n(\mathbf{k})\delta[E_n(\mathbf{k}) - E_F]. \quad (3)$$

where $v_\alpha^n(\mathbf{k}) = dE_n(\mathbf{k})/d\mathbf{k}$ is an α-component of electron velocity in the state $|n, \mathbf{k}>$.

All parameters in Eq. (2), excluding γ, were calculated from first principles taking into account spin polarization and SO coupling. Starting from the calculation of absorptive part of

Table 3. Calculated plasma frequencies (eV).

Compound	$\omega_{p,xx}$	$\omega_{p,yy}$	$\omega_{p,zz}$
CrGaSb	3.64	3.64	3.39
$CrGa_2Sb_2$	2.71	1.45	1.29
$Cr_{0.94}Ga_2Sb_2$[a]	2.12	1.43	1.36

[a] Nonstoichiometric compound.

the dielectric tensor, we then found the dispersive part using the Kramers–Kronig transformation over the energy range 0–21.8 eV. The plasma frequency tensor $\omega^2_{p,\alpha\beta}$ evaluated by (3) for the three compounds is given in Table 3. These data suggest a significant anisotropy of direct-current (dc) conductivity

$$\sigma^{dc}_{\alpha\alpha} = \frac{\omega^2_{p,\alpha\alpha}}{4\pi\gamma} \tag{4}$$

(and, correspondingly, of dc electrical resistivity $\rho^{dc}{}_{\alpha\alpha} = 1/\sigma^{dc}{}_{\alpha\alpha}$) in $CrGa_2Sb_2$ and a nearly isotropic dc conductivity in CrGaSb. A two times higher value of $\omega_{p,xx}$ as compared with $\omega_{p,yy}$ and $\omega_{p,zz}$ means, counterintuitively, that the Fermi electrons in $CrGa_2Sb_2$ move more easily along the *a* axis (actually, along the zigzag —Cr—Ga—Sb— chains) rather than along metallic Cr (**b**, **c**) planes (Fig. 1c). This implies a strong hybridization of Cr 3d-states with 4p- and 5p-states of neighboring Ga and Sb atoms and correlates well with the fact that the Cr 3d-states in $CrGa_2Sb_2$ contribute only 14% to the DOS at the Fermi level $N(E_F)$. A circumstantial evidence of higher conductivity along the *x*-direction in $CrGa_2Sb_2$ is that there are three highly dispersive bands crossing E_F along the Γ–*X* line of BZ *versus* one such band along the Γ–*Y* and Γ–*S* lines [see Fig. 3(right)].

To estimate an anisotropic electrical resistivity $\rho^{dc}{}_{\alpha\alpha}$, we assume that the compounds under study have the relaxation rate of electron scattering $\gamma \approx 0.1$ eV, a value typical of 3d-transition metals at room temperature T_{room}. With this assumption, the resistivity of $CrGa_2Sb_2$ is $\rho^{dc}{}_{xx} = 102$ $\mu\Omega$ cm, $\rho^{dc}{}_{yy} = 354$ $\mu\Omega$ cm, and $\rho^{dc}{}_{zz} = 447$ $\mu\Omega$ cm. If we recall that the Curie temperature of $CrGa_2Sb_2$ (~345–350 K) only slightly exceeds T_{room} and that conduction electrons at T_{room} are strongly scattered by spin fluctuations, then, γ must be several times higher than its typical value of ~0.1 eV. This reasoning leads to $\rho^{dc}{}_{zz}(T_{room}) \sim 1$ mΩ cm and an electron free path length of about two to three interatomic distances. In the case of nonstoichiometric composition $Cr_{0.94}Ga_2Sb_2$, a considerable (~20%) reduction in $\omega_{p,xx}$ indicates a decrease in metallicity with decreasing Cr content. According to (4), such reduction of $\omega_{p,xx}$ suggests that $\rho^{dc}{}_{xx}$ of $Cr_{0.94}Ga_2Sb_2$ increases by a factor of ~1.6, which does not change the qualitative estimate made above for $CrGa_2Sb_2$. A similar estimate for the tetragonal CrGaSb provides $\rho^{dc}{}_{xx} = \rho^{dc}{}_{yy} = 56$ $\mu\Omega$ cm, and $\rho^{dc}{}_{zz} = 65$ $\mu\Omega$ cm, which values are rather high, but not unusual for metallic materials. This result looks quite evident in view of higher Cr concentration in CrGaSb.

The experimental values measured[8] for CrGaSb are $\rho^{dc} = 1.95$ mΩ cm and 2.23 mΩ cm, respectively, at $T = 0$ and 300 K. Noteworthy, the residual resistivity of CrGaSb significantly exceeds the temperature-dependent contribution $\Delta\rho = \rho(300\ K) - \rho(0\ K) = 0.28$ mΩ cm, which suggests a large number of defects in experimental samples. The measured[8] resistivity of $CrGa_2Sb_2$ has huge values $\rho(0\ K) = 0.262$ mΩ cm and $\rho(300\ K) = 0.385$ Ω cm. To reproduce their difference $\Delta\rho = 0.123$ Ω cm using our calculated $\omega_p{}^2$, an unrealistically high relaxation rate $\gamma \geq 28$ eV is required. This suggests the existence of numerous defects in a sample, which radically change its electronic characteristics. We also note that the measured[8] temperature dependence $\rho(T)$ for $CrGa_2Sb_2$ exhibits a peak, which is typical for spin fluctuation scattering near T_C.[24] The peak position $T_{peak} = 290$ K, however, is significantly lower than the Curie temperature of $CrGa_2Sb_2$ (350 K), unlike the case of isostructural phase $MnGa_2Sb_2$, where the cusp position is observed[6] to coincide with $T_C = 310$ K. As the number of defects in samples and their nature are unknown, one should not expect quantitative agreement between theory and experiment. However, our calculations qualitatively correlate with experimental measurements – both compounds have high values of ρ and CrGaSb is more metallic.

With a knowledge of the frequency-dependent dielectric tensor $\varepsilon_{\alpha\beta}(\omega)$, one is able to evaluate the observable optical quantities. Experimentally, most frequently measured quantities are the optical conductivity tensor $\sigma_{\alpha\beta}(\omega)$, normal incidence reflectivity related to the α-polarization of light $R_{\alpha\alpha}(\omega)$, and electron energy loss spectra (EELS) $L_{\alpha\alpha}(\omega)$. These quantities are determined through the dielectric tensor according to the following formulas:

$$\sigma_{\alpha\beta}(\omega) = \sigma_{1,\alpha\beta}(\omega) + \mathrm{i}\sigma_{2,\alpha\beta}(\omega) = \frac{\omega[\varepsilon_{\alpha\beta}(\omega) - \delta_{\alpha\beta}]}{4\pi\,\mathrm{i}}, \tag{5}$$

$$R_{\alpha\alpha}(\omega) = \left|\frac{\sqrt{\varepsilon_{\alpha\alpha}(\omega)} - 1}{\sqrt{\varepsilon_{\alpha\alpha}(\omega)} + 1}\right|^2, \tag{6}$$

$$L_{\alpha\alpha}(\omega) = \mathrm{Im}\left[-\varepsilon^{-1}_{\alpha\alpha}(\omega)\right], \tag{7}$$

where ε^{-1} is the inverse dielectric tensor. Figure 6 displays a diagonal interband optical conductivity $\sigma_{1,\alpha\alpha}(\omega)$ for $CrGa_2Sb_2$ (a) and CrGaSb (b). A significant anisotropy of $\sigma_{1,\alpha\alpha}(\omega)$ in $CrGa_2Sb_2$ is observed in the IR spectral region at $\hbar\omega \sim 0.3$ – 1.0 eV and from 2.0 to 4.0 eV, while at other frequencies the optical conductivity is nearly isotropic. The conductivity of tetragonal phase CrGaSb is appreciably anisotropic from 0 to 2.0 eV and from 3.0 to 4.5 eV and, as a whole, similar to that of $CrGa_2Sb_2$. Figure 7 displays the reflectivity (left) and electron energy loss spectra (right) for $CrGa_2Sb_2$ (with and without Cr vacancies) and CrGaSb. One can see in the figure that $R_{\alpha\alpha}(\omega)$ for all compounds under study is of metallic type (i.e., close to 1) only in the IR region. At $\hbar\omega \sim 0.3$–0.6 eV (depending on light polarization) the reflectivity of $CrGa_2Sb_2$ drastically drops by about one-half, which indicates the onset of intense absorption due to interband electronic transitions. At higher frequencies, $R_{\alpha\alpha}(\omega)$ of $CrGa_2Sb_2$ oscillates between 0.5 and 0.6 remaining nearly isotropic. The absorption edge for CrGaSb is shifted to $\hbar\omega \sim 1.0$ eV, but a general behavior

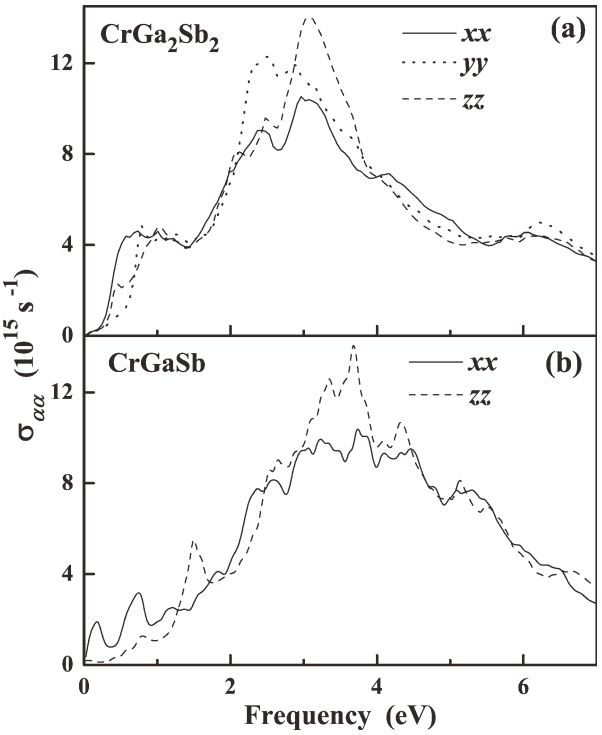

Figure 6. The diagonal interband optical conductivity for (a) $CrGa_2Sb_2$ and (b) CrGaSb.

of reflectivity is rather similar to that of $CrGa_2Sb_2$ (Fig. 7d). Comparison of reflectivity spectra of $CrGa_2Sb_2$ and $Cr_{0.94}Ga_2Sb_2$ (Figs. 7a–7c) shows that in non-stoichiometric case the general shape of $R(\omega)$ is smoothed, and because of this, the absorption edge is shifted toward higher frequencies by 0.1–0.25 eV, depending on light polarization. At $\hbar\omega > 2.0$ eV, the reflectivity spectra of $CrGa_2Sb_2$ and $Cr_{0.94}Ga_2Sb_2$ are similar to each other.

From our calculations it follows that a main peak of $L_{\alpha\alpha}(\omega)$ for $CrGa_2Sb_2$ is several eV wide and centered near 16 eV, which is close to the classical plasma frequency Ω_p equal to 17.1 eV. The value of Ω_p is given by the simple formula $\Omega_p = (4\pi e^2 n_{val}/m)^{1/2}$, where n_{val} is an average density of valence electrons. This formula suggests that valence electrons in a crystal are approximated by the homogeneous electron gas model. In real solids, which have inhomogeneous electron density, the EELS exhibit several additional lower-energy peaks. These peaks of $L(\omega)$ correspond to the dips of reflectivity $R(\omega)$ – they occur at the frequencies, where $R(\omega)$ decreases most rapidly. This correlation between the $R_{\alpha\alpha}(\omega)$ and $L_{\alpha\alpha}(\omega)$ spectra is clearly seen in Figure 7, where they are displayed in the IR and visible spectral region (up to 7 eV) for all the compounds and light polarizations.

The BCO $CrGa_2Sb_2$ is FM, so it may be of interest to calculate its MO properties. As is known, the MO properties are determined by off-diagonal components of the dielectric tensor, which are nonzero in a material with FM magnetization and considerable SO coupling. In the case of $CrGa_2Sb_2$, the SO coupling effects are certainly not small, because this compound contains rather heavy Sb atoms. We calculated the polar MO Kerr effect (MOKE), when the light falls normally to the sample surface and parallel to the direction of magnetization

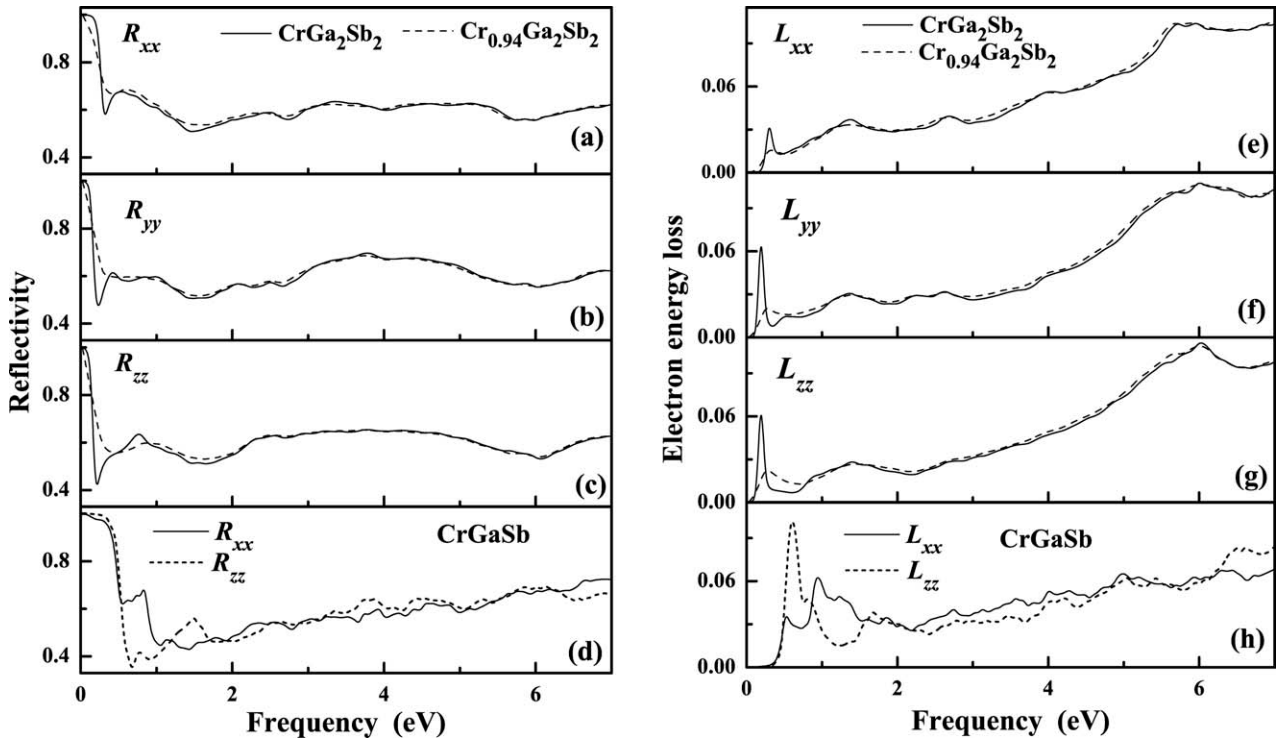

Figure 7. (left) Reflectivity and (right) electron-energy-loss spectra. From the top down: the *xx*, *yy*, and *zz* components for $CrGa_2Sb_2$ (solid line) and $Cr_{0.94}Ga_2Sb_2$ (dashed line). The bottom panels (d, h): the *xx* and *zz* components (solid and dotted lines, respectively) for CrGaSb.

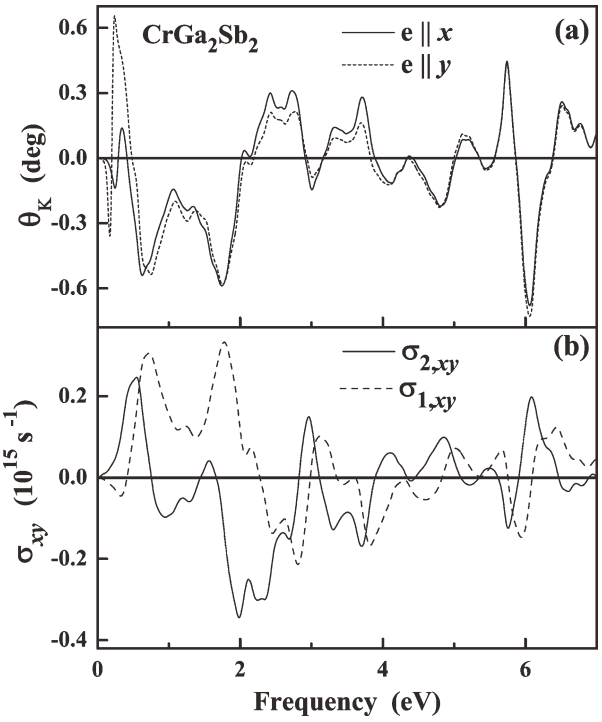

Figure 8. $CrGa_2Sb_2$: a) the Kerr rotation angle for magnetization **M** || **z** and two light polarizations, **e** || **x** (solid line) and **e** || **y** (dots). b) The real (dashed line) and imaginary (solid line) parts of the off-diagonal interband optical conductivity.

M. For this geometry, the Kerr rotation angle $\theta_K(\omega)$ is expressed (to the first order in σ_{xy}) as

$$\theta_K(\omega) \approx \frac{4\pi}{\omega} \mathrm{Re}\left[\frac{-i\sigma_{xy}(\omega)}{\sigma_{xx}(\omega)\sqrt{1+4i\pi\sigma_{xx}(\omega)/\omega}}\right]. \quad (8)$$

Figure 8a shows the Kerr rotation angle $\theta_K(\omega)$ calculated for two light polarizations, **e** || **x** (solid line) and **e** || **y** (dots), with magnetization **M** || **z**. A large Kerr rotation of 0.6°–0.7° is observed near the reflectivity minimum at $\hbar\omega \sim 0.3$ eV, where there is a low-energy plasmon. At this frequency, the incident light penetrates most deeply into a $CrGa_2Sb_2$ sample [this corresponds to a minimum of square root in Eq. (8)], which greatly enhances the efficiency of rotation of a light polarization by the off-diagonal component $\sigma_{xy}(\omega)$. The same explanation is applicable to the region of large $\theta_K(\omega)$ near 6 eV. It should be noted that in general, variations in $\mathrm{Im}[\sigma_{xy}(\omega)]$ with ω (Fig. 8b) turn out to be less important for the frequency dependence of the MOKE than changes in light penetration depth.

Conclusions

The comprehensive *ab initio* study is performed of the new metastable high-pressure phases, tetragonal CrGaSb and orthorhombic $CrGa_2Sb_2$. In addition to the previously published experimental data,[8] the X-ray structural measurements of the phase $CrGa_2Sb_2$ up to 9 GPa are presented. The calculated lattice parameters, equation of state, and high-temperature ferromagnetism of $CrGa_2Sb_2$ are in agreement with available experimental data. The experimentally observed absence of magnetic ordering in CrGaSb and high electrical resistivity of both compounds (with more metallic character of CrGaSb) are also confirmed in our calculations. Calculated optical properties, which are still remain to be explored experimentally, are used to obtain additional information on the electronic structure, type of conductivity, and a degree of metallicity of both compounds. The optical and MO spectra may be helpful for experimental identification of these materials in the future.

Significant discrepancies between theory and experiment are found for the total magnetic moment (calculated value is by ~20% higher) and absolute value of electrical conductivity in $CrGa_2Sb_2$. In this context, noteworthy is the pseudogap of 0.2–0.3 eV around the Fermi level in $CrGa_2Sb_2$ observed in our electronic structure calculations, the feature typical of poor metals. As our calculations were made at the experimental lattice parameters, we checked how sensitive were the electronic and magnetic properties of $CrGa_2Sb_2$ to variations in the cell volume, and found that on compression up to 9 GPa the magnetic moment was reduced by only 6%, while the DOS at E_F does not actually change.

Two other possible reasons for the discrepancies between theoretical and experimental results were studied, namely, the role of reported[7] small Cr deficiency and the effect of particular exchange–correlation potential. The calculated DOS, plasma frequencies, and reflectivity spectra reveal that the nonstoichiometric compound $Cr_{0.94}Ga_2Sb_2$ with ~6% of Cr vacancies is less metallic compared to perfect $CrGa_2Sb_2$. Nevertheless, the small Cr deficiency does not bring this system to a semiconducting state. The DOS at E_F and magnetic properties are not profoundly altered in the presence of Cr vacancies.

We also compared the results for $CrGa_2Sb_2$ obtained using the LDA, GGA, and new MBJ[16] exchange–correlation potentials. The magnetic moment of $CrGa_2Sb_2$ is found to be not very sensitive to the type of exchange–correlation potential. As for the electronic structure, in going from LDA to GGA and then to MBJ, the DOS at E_F becomes lower and pseudogap wider, however, $CrGa_2Sb_2$ is not semiconducting. In the case of MBJ potential, the DOS at E_F is by a factor of 1.8 smaller than in our standard DFT calculations. Based on the estimate of the Thomas–Fermi screening length for $CrGa_2Sb_2$, we conclude that this compound is characterized by the short-range self-energy, so significant deviations from the DFT results should not be expected. Most noteworthy is that in the MBJ calculation the DOS of spin-up electrons at 0.2 eV above E_F is nearly zero. If due to some reason (doping, disorder, compression, etc.) the Fermi level of $CrGa_2Sb_2$ was at this energy, this compound would be very close to half-metallic behavior. This observation is consistent with almost integer magnetic moment ($\approx 2\ \mu_B$/Cr) of $CrGa_2Sb_2$, which is characteristic of half-metallic ferromagnets.

We would like to mention another plausible explanation of the experimentally observed[8] high electrical resistivity in $CrGa_2Sb_2$. We mean the possible formation of a long-period superstructure, which, under certain conditions, might provide a band gap in the corresponding direction of BZ, resulting in

additional degradation of metallic properties. This suggestion is to some extent supported by recent X-ray and SEM studies of the related system Mn–GaSb, where superstructure reflexes, weak as they are, have been observed.[25] However, this finding still remains to be confirmed by other independent studies, such as neutron scattering measurements.

To conclude, our first-principles calculations demonstrate that CrGaSb and $CrGa_2Sb_2$ are rather poor metals. The analysis of calculation results does not confirm the assumption[8] of semiconducting properties of $CrGa_2Sb_2$. Nevertheless, the existence of pseudogap in the electronic spectrum, as well as the half-metallic feature in the DOS curve just above the Fermi level, imply that at certain conditions and/or after a special treatment (thermal processing, compression, doping, etc.) a semiconducting or half-metallic state in the system Cr–GaSb can be achieved. Thus, we consider the FM phase $CrGa_2Sb_2$ and other compounds of this class as a promising basis for the search of novel spintronics-related materials.

Acknowledgments

The numerical calculations are performed at the Joint Supercomputer Center of RAS and the Supercomputing Center of Russian Research Centre "Kurchatov Institute."

Keywords: electronic structure · magnetic materials · conductivity · high-pressure · vacancies · optical properties

How to cite this article: E. Kulatov, M. Magnitskaya, Y. Uspenskii, S. Popova, V. Brazhkin, E. Maksimov, *Int. J. Quantum Chem.* **2012,** DOI: 10.1002/qua.24097

[1] S. A. Wolf, D. D. Awschalom, R. A. Buhrman, J. M. Daughton, S. von Molnár, M. L. Roukes, A. Y. Chtchelkanova, D. M. Treger, *Science* **2001**, *294,* 1488.
[2] Y. Ohno, D. K. Young, B. Beschoten, F. Matshkura, H. Ohno, D. D. Awschalom, *Nature* **1999**, *402,* 790.
[3] A. M. Nazmul, T. Amemiya, Y. Shuto, S. Sugahara, M. Tanaka, *Phys. Rev. Lett.* **2005**, *95,* 017201.
[4] S. V. Popova, O. A. Sazanova, V. V. Brazhkin, N. V. Kalyaeva, M. V. Kondrin, A. G. Lyapin, *Phys. Solid. State* **2006**, *48,* 2177.
[5] M. V. Kondrin, S. V. Popova, V. P. Gizatullin, O. A. Sazanova, N. V. Kalyaeva, A. G. Lyapin, V. V. Brazhkin, S. A. Gudoshnikov, Y. V. Prokhorova, *JETP Lett.* **2006**, *84,* 195.
[6] W. Sakakibara, Y. Hayashi, H. Takizawa, *J. Ceram. Soc. Jpn.* **2009**, *117,* 72.
[7] W. Sakakibara, Y. Hayashi, H. Takizawa, *J. Alloys Compd.* **2010**, *496,* L14.
[8] M. V. Kondrin, V. P. Gizatullin, S. V. Popova, A. G. Lyapin, V. V. Brazhkin, V. Y. Ivanov, A. A. Pronin, Y. B. Lebed, R. A. Sadykov, *J. Phys. Condens. Matter* **2011**, *23,* 446001.
[9] E. T. Kulatov, M. V. Magnitskaya, E. G. Maksimov, A. A. Titov, Y. A. Uspenskii, *EPL* **2011**, *96,* 27009.
[10] (a) P. Hohenberg, W. Kohn, *Phys. Rev.* **1964**, *136,* B864; (b) W. Kohn, L. J. Sham, *Phys. Rev.* **1965**, *140,* A1133.
[11] P. Blaha, K. Schwarz, G. K. H. Madsen, D. Kvasnicka, J. Luitz, In WIEN2k: An Augmented Plane Wave + Local Orbitals Program for Calculating Crystal Properties; K. Schwarz, Ed.; Technische Universität Wien: Vienna, **2011**; pp. 1–223. http://www.wien2k.at/ (accessed Jan. 25, 2012).
[12] D. M. Ceperley, B. J. Alder, *Phys. Rev. Lett.* **1980**, *45,* 566.
[13] J. P. Perdew, Y. Wang, *Phys. Rev. B* **1992**, *45,* 13244.
[14] J. P. Perdew, K. Burke, M. Ernzerhof, *Phys. Rev. Lett.* **1996**, *77,* 3865.
[15] A. D. Becke, E. R. Johnson, *J. Chem. Phys.* **2006**, *124,* 221101.
[16] F. Tran, P. Blaha, *Phys. Rev. Lett.* **2009**, *102,* 226401.
[17] S.-D. Guo, B.-G. Liu, *EPL* **2011**, *93,* 47006.
[18] D. D. Koelling, B. N. Harmon, *J. Phys. C Solid State Phys.* **1977**, *10,* 3107.
[19] A. V. Tsvyashchenko, L. N. Fomicheva, M. V. Magnitskaya, V. A. Sidorov, E. N. Shirani, A. V. Kuznetsov, D. V. Eremenko, V. N. Trofimov, *Phys. Met. Metallogr.* **2002**, *93,* S59.
[20] Uspenskii, A. Yu, E. T. Kulatov, *J. Magn. Magn. Mater.* **2009**, *321,* 931.
[21] L. G. Khvostantsev, V. N. Slesarev, V. V. Brazhkin, *Int. J. High Pressure Res.* **2004**, *24,* 371.
[22] K. Schwarz, P. Mohn, *J. Phys. F Met. Phys.* **1984**, *14,* L129.
[23] L. Hedin, S. Lundqvist, In Solid State Physics, Vol. *23; H. Ehrenreich, F. Seitz, D. Turnbull, Eds.; Academic Press: New York,* **1969**; p. 1.
[24] M. Kataoka, *Phys. Rev. B* **2001**, *63,* 134435.
[25] O. A. Sazanova, S. V. Popova, M. V. Kondrin, V. V. Brazhkin, A. G. Lyapin, N. F. Borovikov, I. P. Zibrov, T. I. Dyuzheva, N. B. Bolotina, In Abstr. IX Conf. on Strongly Correlated Electron Systems and Quantum Critical Phenomena, Troitsk, Moscow Region, June 9, **2011**.

Received: 29 January 2012
Revised: 29 January 2012
Accepted: 1 March 2012
Published online on Wiley Online Library